Nanoscale

PAPER

View Article Online
View Journal | View Issue

Cite this: *Nanoscale*, 2017, **9**, 2845

Fully alloyed metal nanorods with highly tunable properties†

Wiebke Albrecht,*‡[a] Jessi E. S. van der Hoeven,‡[a,b] Tian-Song Deng,[a] Petra E. de Jongh[b] and Alfons van Blaaderen*[a]

Received 29th October 2016,
Accepted 16th January 2017

DOI: 10.1039/c6nr08484b

rsc.li/nanoscale

Alloyed metal nanorods offer a unique combination of enhanced plasmonic and photothermal properties with a wide variety in optical and catalytic properties as a function of the alloy composition. Here, we show that fully alloyed anisotropic nanoparticles can be obtained with complete retention of the particle shape *via* thermal treatment at surprisingly low temperatures. By coating Au–Ag, Au–Pd and Au–Pt core–shell nanorods with a protective mesoporous silica shell the transformation of the rods to a more stable spherical shape was successfully prevented during alloying. For the Au–Ag core–shell NRs the chemical stability was drastically increased after alloying, and from Mie–Gans and finite-difference time-domain (FDTD) calculations it followed that alloyed AuAg rods also exhibit much better plasmonic properties than their spherical counterparts. Finally, the generality of our method is demonstrated by alloying Au–Pd and Au–Pt core–shell NRs, whereby the AuPd and AuPt alloyed NRs showed a surprisingly high increase in thermal stability of several hundred degrees compared with monometallic silica coated Au NRs.

Introduction

Confining electrons in metals to the nanoscale leads to efficient interactions with light due to localized surface plasmon resonance (LSPR) which gives rise to interesting optical and photothermal properties. Unlike spherical particles, nanorods (NRs) have two LSPRs: a transverse and longitudinal resonance. The longitudinal LSPR can be tuned by changing the aspect ratio and spans the visible to the near-infrared (NIR) region of the spectrum. Metal NRs also exhibit better plasmonic properties and stronger local field enhancements than nanospheres, making them valuable materials for light-based applications. Due to their strong plasmon resonance and chemical stability, Au NRs are successfully employed in many applications such as optical data storage,[1] photocatalysis,[2] sensing[3] and cancer treatment.[4,5]

Of all metals Ag shows the best plasmonic properties due to a low imaginary part of its dielectric function over a large energy region. By growing a silver shell around Au nanoparticles (NPs), the plasmonic properties can be significantly enhanced,[6,7] but their applicability is hampered by the relatively poor chemical stability of the Ag shell. Alloying the two metals solves this problem as it significantly increases the chemical stability of the particles, which was shown for spherical NPs.[7] Furthermore it leads to additional control over optical properties.[8]

Alloyed metal NPs are also interesting for catalysis,[9,10] as their catalytic properties can be superior to the single-component systems.[11,12] Irradiating such metal catalysts with light can enhance their catalytic performance due to their plasmonic properties.[2,13] In addition, alloying can lead to a significant increase in the thermal stability of the NPs.[14,15]

Ideally one would like to combine the superior rod-shape with the advantages of alloyed materials. However, there is no facile way of making rod-shaped alloys while simultaneously controlling their composition and shape, and most studies to date have focused on spherical alloyed NPs. Only a few examples were reported on the synthesis of alloyed NRs, such as template-directed electro-chemical or wet-chemical co-deposition and low-temperature decomposition of bimetallic precursors.[16–21] These synthesis routes only yield NRs with a fixed composition and/or are highly laborious with small amounts of sample obtained. Alternatively, alloying of spherical core–shell nanoparticles *via* thermal treatment is a simple and scalable method with precise control over composition

[a]*Soft Condensed Matter, Debye Institute for Nanomaterials Science, Utrecht University, Princetonplein 5, 3584 CC Utrecht, The Netherlands. E-mail: W.Albrecht@uu.nl, A.vanBlaaderen@uu.nl*

[b]*Inorganic Chemistry and Catalysis, Debye Institute for Nanomaterials Science, Utrecht University, Universiteitsweg 99, 3584 CG Utrecht, The Netherlands*

†Electronic supplementary information (ESI) available: Details of methods, the influence of time and electron beam on *in situ* heating of Au@Ag@SiO_2 NRs, EDX map of silica coating and etched NRs, calculated extinction spectra of alloyed NRs for varying aspect ratios, deformation due to Ag loss, heating of monometallic NRs, *in situ* heating of Au@Pt@SiO_2 NRs. See DOI: 10.1039/C6NR08484B

‡These authors contributed equally to this work.

and size.[7,22] Unfortunately, at the elevated temperatures required for alloying, the rod-shape is unstable and the rod deforms to a spherical shape.[23] A protective coating can improve the stability during heat treatment and was used for making spherical alloyed NPs.[7] However, it has not been shown yet that this method can be extended to anisotropic particles without changing the particle shape after alloying and how an out-of equilibrium NR shape influences this process.

Here we make, for the first time, fully alloyed nanorods *via* thermal treatment while retaining the anisotropic particle shape. This is achieved by coating the particles with a protective mesoporous-silica layer, which enhances their thermal stability, prevents sintering of NRs during thermal treatment and allows mass transport to the metal surface, which is crucial for catalytic applications. Surprisingly, alloying was achieved at much lower temperatures than needed to alloy spherical NPs as reported by Gao *et al.*[7] implying that the out-of equilibrium shape of NRs could play an important role. The metal composition of the NRs can be tuned precisely by varying the core-to-shell size ratio.[6] In this study, we followed the alloying of mesoporous-silica coated Au(core)–Ag(shell) nanorods (Au@Ag@SiO_2 NRs), Au(core)–Pd(shell) nanorods (Au@Pd@SiO_2 NRs) and Au(core)–Pt(shell) nanorods (Au@Pt@SiO_2 NRs) *in situ* with high-angle annular dark field scanning transmission electron microscopy (HAADF-STEM) and energy-dispersive X-ray spectroscopy (EDX). We compared the measured extinction spectra of AuAg alloyed NRs with an empirically shape-corrected analytical model based on the Mie–Gans theory and with FDTD calculations, and found enhanced plasmonic properties of the alloyed NRs over their spherical counterparts. Moreover, the thermal stability of the alloyed NRs was greatly improved. It is important to stress that our methodology is not limited to the metals chosen in this paper or to rod-shaped nanoparticles, but can be applied to different metals and different anisotropic particle shapes as well.

Methods

Synthesis, alloying and stability experiments

The Au@Ag@SiO_2, Au@Pd@SiO_2 and Au@Pt@SiO_2 core–shell NRs were synthesized according to ref. 6. To form alloys, these particles were heated either *in situ* in an electron microscope using a heating stage or externally in a furnace under an air or N_2 atmosphere. For the *in situ* heating the particles were dropcast on a SiN heating chip and inserted in an electron microscope. The temperature was changed in steps of 50 °C (5 min heating at a constant temperature) and the changes were monitored using STEM and EDX (15 minutes at a constant temperature). For the oven heating experiments the particles were dropcast on a microscope glass slide and heated at 400 °C for 30 min (air) and 60 min (N_2). The extinction spectra before and after heating were measured with Fourier transform infrared spectroscopy (FTIR) on the particles on a microscope slide in an air environment. Our Bruker Vertex 70 spectrometer is equipped with a NIR source, a quartz beam splitter and a Si diode detector, which enabled us to measure in the VIS as well. To check the chemical stability, the Au@Ag@SiO_2 core–shell and AuAg@SiO_2 alloyed particles on the microscope slide were exposed to an aqueous mixture of 1.7 vol% H_2O_2 and 0.9 vol% $NH_3{\cdot}H_2O$ for 15 min and 2 h, respectively. More experimental details about equipment, chemicals and procedures can be found in the ESI.†

Calculations

We calculated the extinction spectra for the alloyed spherical NPs and NRs with FDTD simulations or Mie theory and Mie–Gans theory, respectively. Mie–Gans theory is only valid for spheroidal shapes, and to adapt it to experimentally more realistic particle shapes, an empirical shape correction factor was used based on the experimentally obtained aspect ratio and volume.[24] For the spherical particles the same volume was assumed as for the NRs. We took the dielectric functions from an analytical model derived from measurements of the dielectric function of certain alloy compositions, which allows for extrapolation of the dielectric function to any composition.[8] It is important to use dielectric functions obtained for alloys as it was demonstrated that the measured extinction spectra of spherical AuAg alloyed NPs could not be reproduced by a linear combination of the dielectric functions of Au and Ag but only by using the dielectric data of alloys.[8,25] We furthermore size-corrected the dielectric functions to account for the influence of the particle size confinement on the electron mean free path.[26] A detailed description of the calculations can be found in the ESI.†

Results and discussion

To study the thermally induced alloying of nanorods we first synthesized Au@Ag NRs in a mesoporous silica shell.[6] The average length of the Au@Ag rods was 73 nm and the diameter was 27 nm, while the Au core length and diameter were 61 nm and 20 nm, respectively. In order to find the required heating temperature for alloying which can deviate substantially from bulk values,[22,27] the core–shell NRs were heated *in situ* in a high-resolution electron microscope operated in HAADF-STEM mode. The temperature was increased in 50 °C steps and kept constant for 5 min at each temperature (Fig. 1). Below 400 °C the Au core and Ag shell can clearly be distinguished by the *z*-contrast inherent to STEM. At 400 °C this contrast difference became less apparent and vanished at 450 °C indicating that an alloy was formed. The EDX measurements in Fig. 1b show that alloying started at the Au–Ag interface at 400 °C and confirmed the transition of the core–shell structure to a homogeneous alloy at 450 °C. After cooling back to room temperature, the alloyed structure was preserved (Fig. 1b) and the FCC crystallinity of the rod retained (Fig. 2), as expected for AuAg alloys. The (111) lattice spacing of a formed AuAg alloy NR was measured to be 0.235 nm in good agreement with the known values of 0.2355 nm and 0.2358 nm for Au and Ag FCC

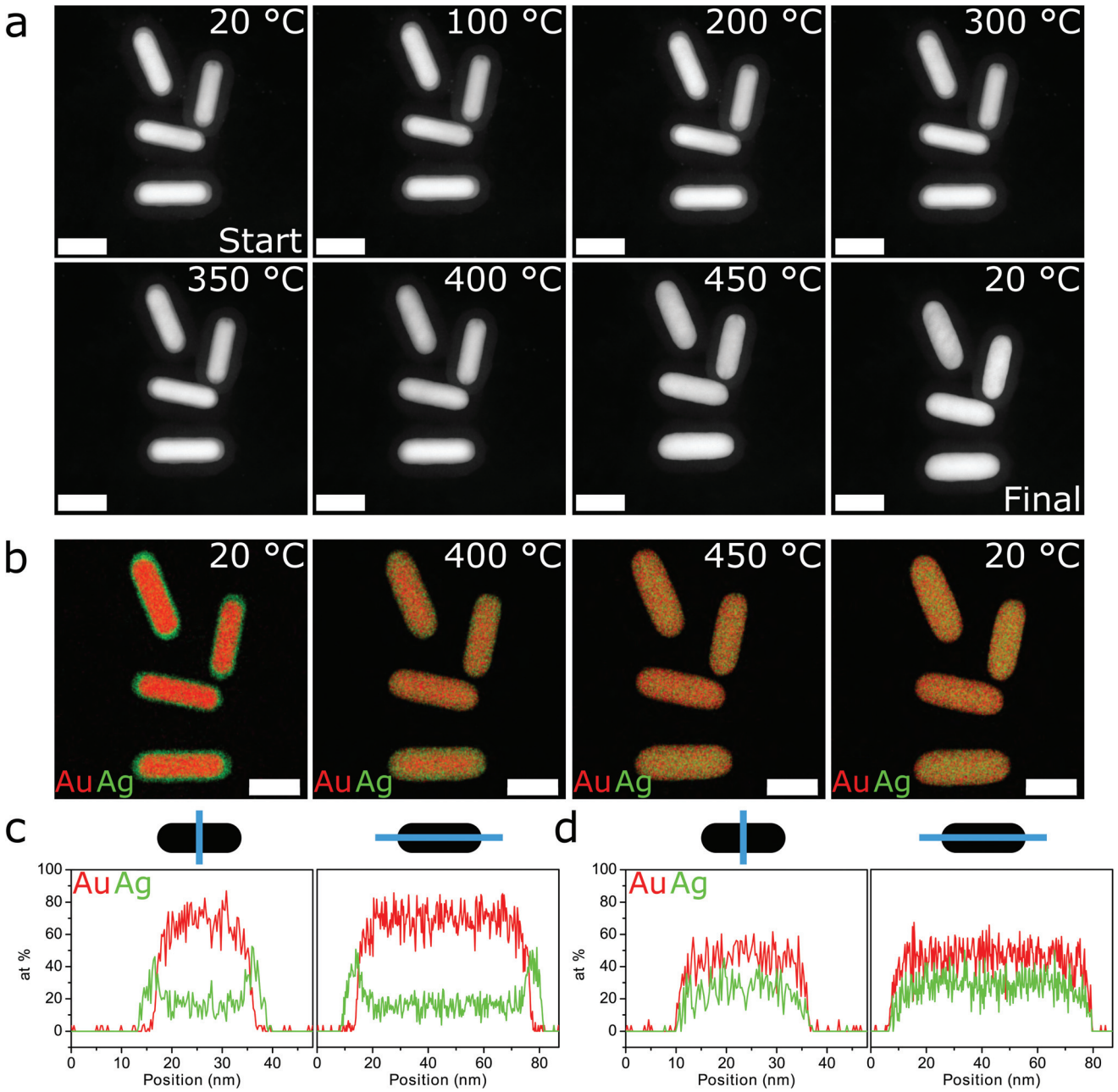

Fig. 1 *In situ* heating of silica coated Au@Ag core–shell nanorods. (a) HAADF-STEM images recorded before, during and after heating to 450 °C. The scale bars are 50 nm. (b) EDX maps showing the metal distribution of Ag (green) and Au (red) in the core–shell and alloyed metal nanorods before and after heating, respectively. The average aspect ratio of the four particles shown here changed from 3.0 to 2.7 when heated to 450 °C. All scale bars are 40 nm. (c) EDX line scans perpendicular and along the long axis of the top left nanorod at 20 °C and (d) 450 °C. It should be mentioned that the SiO_2 shell is always present (Fig. S8†) although the Si or O EDX maps are not shown here and the SiO_2-STEM contrast is weak compared to the metals.

crystals, respectively. The particles preserved their anisotropic shape during heat treatment due to the stabilizing silica shell. The same Au–Ag ratio was obtained before and after heating, which was approximately 57/43 as determined from EDX. To make sure that alloying was not induced by the electron beam, we checked different spots that had not been exposed to the electron beam prior to heating (Fig. S7†) and concluded that the alloying was not modified by the electron beam.

It needs to be mentioned that it is remarkable that alloying was achieved at such low temperatures which are well below the bulk melting temperatures of Au and Ag. For spherical NPs, Gao *et al.* needed to heat to at least 930 °C to obtain fully alloyed AuAg NPs.[7] Similarly to the volume dependent thermal stability of nanoparticles, an effect that is mainly relevant for sizes below 10 nm,[28–31] smaller particle volumes could be expected to alloy at lower temperatures. However, the decrease

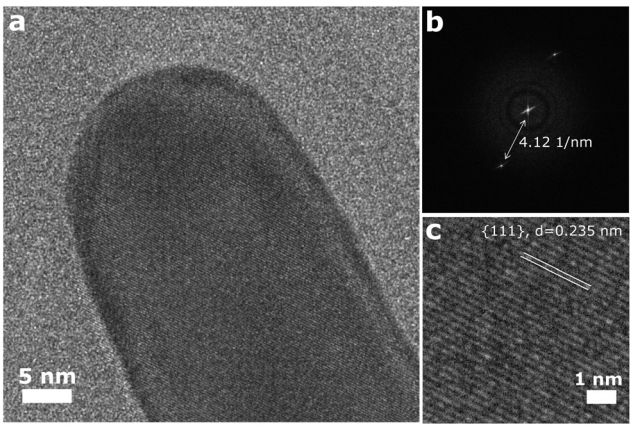

Fig. 2 High-resolution electron microscopy of an alloyed NR. (a) High resolution TEM image, (b) the corresponding FFT and (c) zoom in of an AuAg@SiO_2 alloyed nanorod (L = 74 nm, D = 27 nm, AR = 2.7) after *in situ* heating showing showing the {111} lattice planes with a lattice spacing of 0.235 nm.

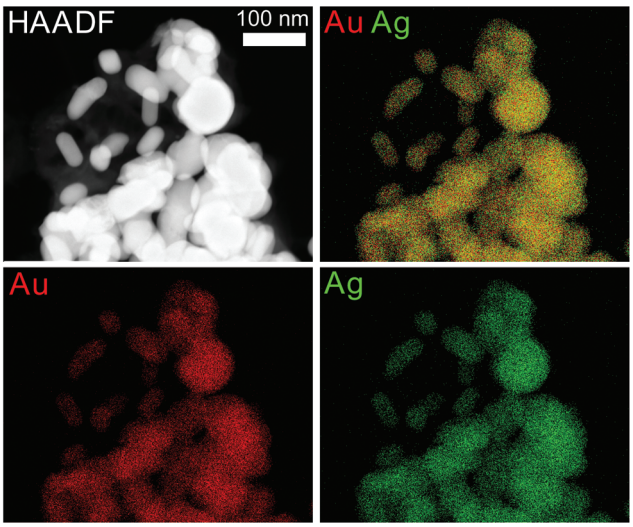

Fig. 3 STEM image and EDX intensity maps of initial Au@Ag core–shell NRs without a mesoporous silica shell after heating them for 1 h at 400 °C in N_2.

in alloying temperature cannot be ascribed to a smaller particle volume in this case, since our rods have a 6.6 × larger volume than the spherical particles used by Gao *et al.* Also a difference in Au–Ag interface area can hardly explain the temperature difference since the rods and spheres have a comparable interface-to-volume ratio of 0.13 nm^{-1} and 0.10 nm^{-1}, respectively. This implies that alloying for out-of equilibrium shaped particles like NRs is quite different from equilibrium processes. Such out-of equilibrium behaviour was, for example, also observed in the thermal deformation of Au NRs towards more spherical shapes which happens at temperatures far below the melting point of Au.[23]

Alloying of larger quantities of Au@Ag@SiO_2 NRs was successfully achieved outside the electron microscope in an oven. We observed a strong effect of the surrounding atmosphere on the alloying process when heating the NRs to 400 °C. The EDX maps in Fig. 4a demonstrate that alloyed NRs were formed during heating in nitrogen. The blue-shift in the extinction spectrum after alloying is mainly due to a slight decrease in aspect ratio and is in agreement with our calculations (Fig. S4†). Identically to the *in situ* experiments, the particles heated externally kept their rod shape, which would not be possible without the protecting silica shell.[23,32,33] We demonstrate this in Fig. 3 where we show results of the heated Au@Ag core–shell NRs (L = 84 nm, D = 24 nm, AR = 3.5) that were not protected by a mesoporous silica shell. As expected, the nanorod shape could not be preserved and the particles deformed and sintered together.

We furthermore demonstrate the enhanced chemical stability of the obtained alloyed NRs. We exposed both the silica-coated core–shell and alloyed NRs to a mixture of hydrogen peroxide (H_2O_2) and ammonia (NH_3), which is known to oxidize and dissolve Ag.[7] The longitudinal LSPR peak of the core–shell particles dropped to about 40% of the original value and red-shifted after only 15 min (Fig. 4c). This indicates that the Ag shell was dissolved as confirmed by our EDX measurements (Fig. S9†). Indeed a similar but reverse shift and increase in intensity were observed when Ag was grown onto the Au rod (Fig. S1†). Contrarily, the peak position and Au–Ag ratio of the alloyed NRs did not change after keeping the particles in the etch solution for 2 h (Fig. 4c).

The situation is very different when heating Au@Ag@SiO_2 NRs in air. The larger blue-shift in the extinction spectrum in Fig. 4b upon heating, compared with heating under nitrogen flow, can only be explained by the deformation of the rods to a more spherical shape. The EDX and STEM images confirm that the particles heated in air deformed. The average aspect ratio dropped from 2.7 (73 nm × 27 nm) to 1.7 (42 nm × 25 nm) with an average volume loss of almost 50%. Interestingly, the EDX measurements revealed that most of the Ag vanished after heating, which explains the observed volume loss, leaving a void for the Au to deform towards the thermodynamically more stable spherical shape (see also Fig. S11†). The difference in the behaviour of the Ag shell during inert and oxygen rich heat treatment is probably linked to the oxidation state of the silver. Heating of Ag NPs on silica supports in air was reported to give similar losses of silver and was ascribed to the dissolution of silver ions in the silica support.[34]

To compare the experimental results with theoretical predictions and to explore a larger parameter space in composition and aspect ratio, we performed FDTD simulations and calculations based on the Mie–Gans theory which we tailored for our experimental shapes and corrected for size-confinement of the electrons (see the ESI† for details). As displayed in Fig. 5a, the LSPR can be tuned by changing the composition of the alloyed NR, similarly as for spherical particles. Most compositions show comparable extinction intensities to those of a pure Au NR, although around an Ag composition of x_{Ag} = 0.5 the intensities are slightly decreased, caused by the dielectric

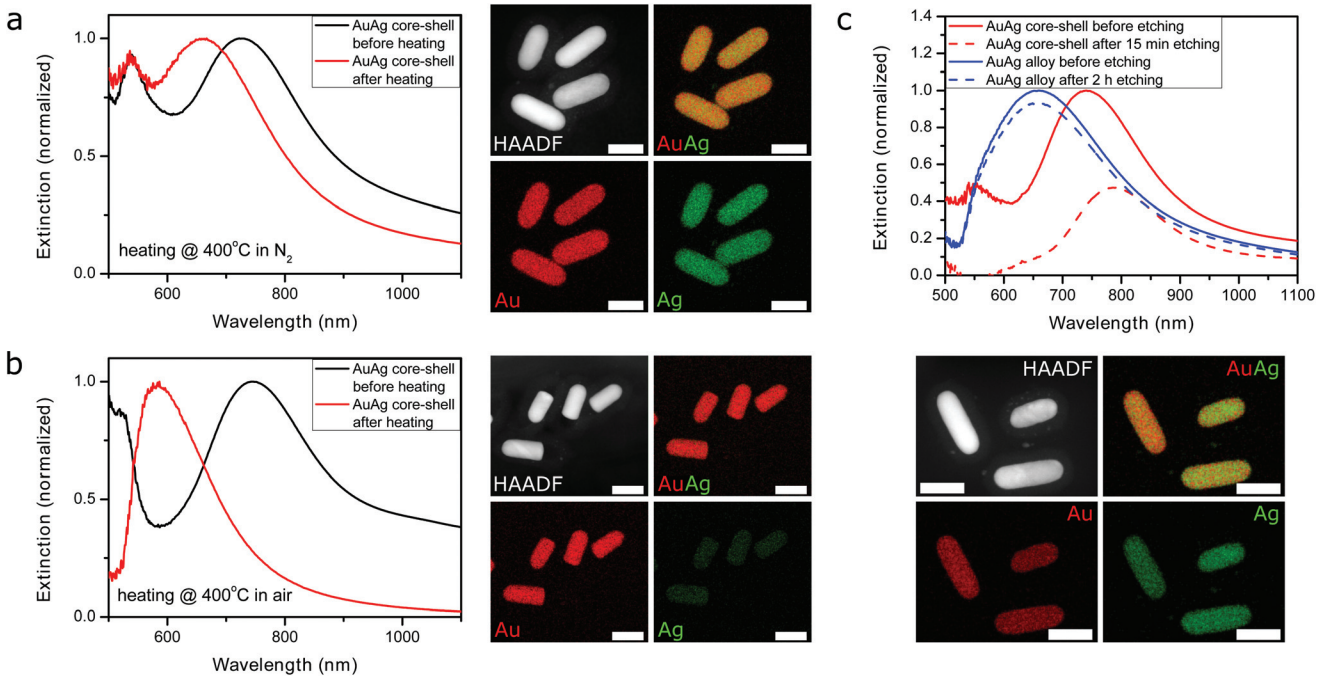

Fig. 4 Alloying of silica coated Au@Ag core–shell nanorods in different gas atmospheres and increased chemical stability against etching of AuAg alloyed NRs. (a) Extinction spectra of AuAg nanorods before (black) and after heat treatment (red) under a N_2 atmosphere and (b) under an air atmosphere show a LSPR peak shift from 740 to 667 nm and from 745 to 586 nm, respectively. The HAADF-STEM image and EDX maps show homogeneously mixed Au(red)–Ag(green) nanorods after heating in N_2 and deformed rods that lost most of the silver after heating in air. The average aspect ratio of the four particles shown in (a) and (b) are 2.4 and 2.1, respectively. The Au–Ag ratio after heat treatment in N_2 was 56/44 whereas after heating in air Ag loss occurred and the Au–Ag ratio shifted to 79/21. The scale bars are 40 nm. (c) Extinction spectra of core–shell (red) and alloyed (blue) nanorods before (solid) and after (dotted) exposure to an aqueous etching solution (1.7 vol% H_2O_2 and 0.9 vol% NH_3 solution). The EDX maps show alloyed nanorods after 2 h of etching. The scale bars are 50 nm.

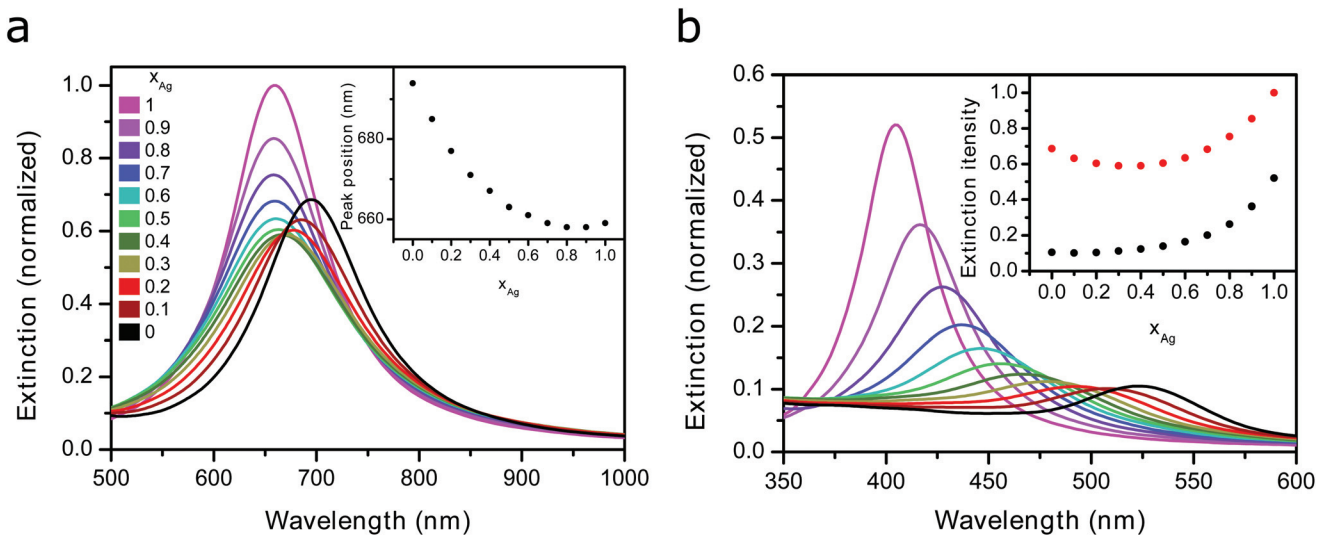

Fig. 5 Comparison of calculated extinction spectra of AuAg alloyed rods and spheres of the same volume. (a) FDTD calculations for AuAg alloyed NRs with a cylindrical shape with varying composition. The inset shows the extinction peak position as a function of Ag composition. (b) FDTD calculations for spherical AuAg alloyed particles of the same volume as the NRs in (a). The inset compares the extinction intensities of the rods (red) with the spheres (black) normalized to the extinction intensity of the Ag NR.

functions of the alloys exhibiting higher losses close to 50% composition than the pure metals (Fig. S3†). The plasmonic properties improve when more Ag is added and exceed those of pure gold at $x_{Ag} = 0.7$. For comparison we added the calculated extinction spectra for alloyed spherical particles of the same volume in Fig. 5b. It needs to be mentioned that the

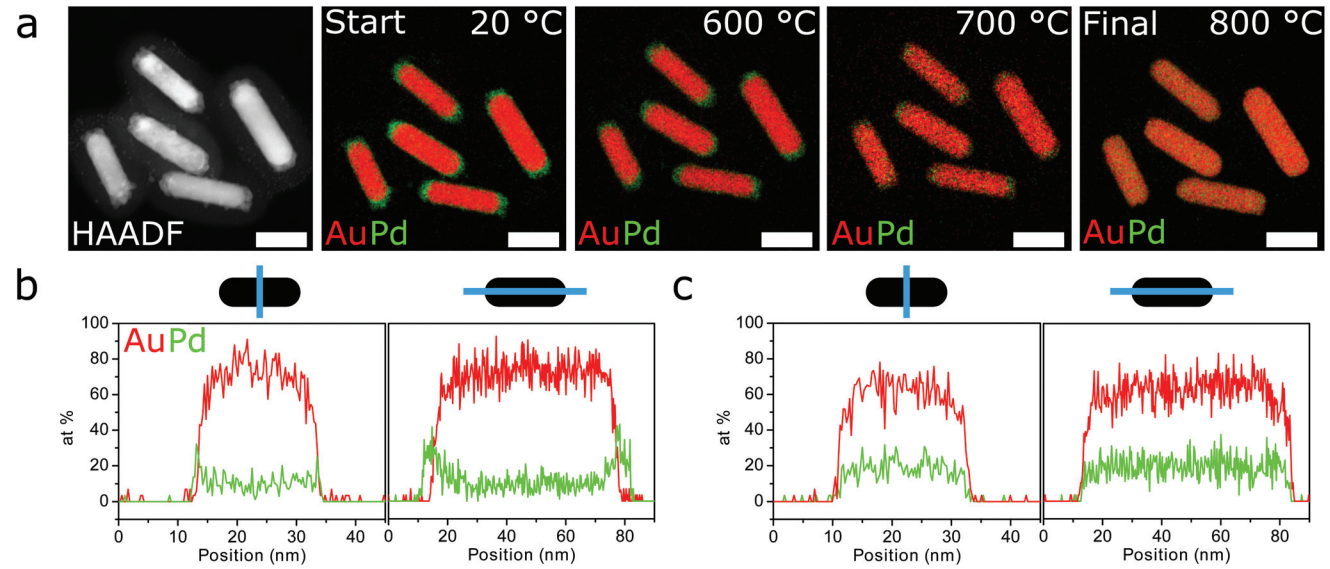

Fig. 6 *In situ* heating of silica coated Au@Pd core–shell nanorods. (a) HAADF-STEM image and EDX maps showing the Au (red) and Pd (green) metal distribution before and during heating to 800 °C, respectively. The average aspect ratio of the five particles shown here changed from 3.3 to 3.2 when heating to 800 °C. The scale bars are 40 nm. (b) EDX line scan of the most right AuPd nanorod at 20 °C and 800 °C.

plasmon wavelengths of the pure Ag and Au spherical NP are slightly blue-shifted as known from the measurements done in water since our used surrounding medium dielectric constant is lower (1.65) than that of water (1.77) to mimic our experimental conditions. The alloyed NRs show improved plasmonic properties compared with spherical particles with up to 9 times higher extinction coefficients. The enhancement can even be increased up to 14 times when using larger aspect ratios (Fig. S10†). These findings were also confirmed by the Mie–Gans calculations which gave results very similar to the FDTD calculations shown in Fig. 3 (Fig. S5†). Both methods could reproduce the measured extinction spectra from Fig. 4a which is presented in Fig. S6.† Thus, alloyed AuAg NRs have significantly better plasmonic and hence photothermal properties than their spherical counterparts.

Our method for the alloying of core–shell rods can, in principle, be applied to any combination of metals that mix in the bulk phase. As a proof of principle *in situ* heating measurements of Au@Pd@SiO_2 NRs with an average length of 73 nm, diameter of 22 nm and Au–Pd ratio of 69/31 (Fig. 6) and of Au@Pt@SiO_2 NRs with an average length of 57 nm, diameter of 18 nm and Au–Pt ratio of 85/15 (Fig. S13†), were carried out. Fig. 6 shows that the initially dendritic Pd shell first smoothened around 500 °C, then started to mix with the Au core at 700 °C and finally formed a homogeneous alloy when heated for about 30 min at 800 °C. We found indications that the alloying temperature depends on the metal ratio as for a lower Pd content alloying was achieved at 600 °C (not shown). Similarly to the observed alloying temperatures for the AuAg NRs, the observed temperatures for AuPd and AuPt are far below the bulk melting temperatures of Au, Pd and Pt.

Remarkably, the AuPd and AuPt NRs did not seem to lose any anisotropy during the heating process, whereas pure Au NRs deform at such high temperatures, even with a silica-coating[32] (Fig. S12†). Hence, alloying Au with a relatively small amount of Pd or Pt (that have significantly higher melting temperatures) can drastically increase the thermal stability of the rod. The combination of the good optical properties of Au and the enhanced thermal and catalytic properties of Pd/Pt make alloyed AuPd/Pt rods interesting materials for, for example, photocatalysis,[13,35] optical laser writing[36] or other applications where the dynamic range is limited by the thermal stability of the NRs.[4,5]

Conclusions

In conclusion, we introduced a general approach to obtain alloyed metallic NRs in a mesoporous silica shell of which the metal composition and optical properties can be tuned. The silica coating provides both thermal and colloidal stability, whereas its mesoporosity enables mass transport to the NR surface during, for example, catalysis.[37] Interestingly, alloying was achieved at much lower temperatures than needed to alloy spherical NPs,[7] which is ascribed to the out-of equilibrium shape of the NR. We furthermore showed that the plasmonic properties of the resulting NRs were enhanced compared with spherical particles of the same volume, and that thermal stability can be greatly improved by alloying with higher melting point metals. We expect that our method can be employed with any combination of metals that mix in the bulk phase. Furthermore, it is possible to extend this method to more than two metals or to different anisotropic particle shapes. Thus, our research opens the way to a wide variety of anisotropic nano-alloys with variable compositions, tunable properties

and different particle shapes which would be difficult to achieve *via* direct synthesis routes.

Acknowledgements

We thank Tom A. J. Welling for discussion about the Mie–Gans calculations and Marijn A. van Huis for facilitating the *in situ* heating electron microscopy measurements. We furthermore thank Chris L. Kennedy, Richard Bintanja and Laura Filion for critical reading of the manuscript. The authors acknowledge financial support from the European Research Council under the European Unions Seventh Framework Programme (FP-2007–2013)/ERC Advanced Grant Agreement #291667 HierarSACol, the Foundation of Fundamental Research on Matter (FOM) and the Netherlands Organization for Scientific Research (NWO-Vici, 724.012.001).

References

1 P. Zijlstra, J. W. M. Chon and M. Gu, *Nature*, 2009, **459**, 410–413.
2 S. Linic, U. Aslam, C. Boerigter and M. Morabito, *Nat. Mater.*, 2015, **14**, 567–576.
3 L. Vigderman, B. P. Khanal and E. R. Zubarev, *Adv. Mater.*, 2012, **24**, 4811–4841.
4 L. C. Kennedy, L. R. Bickford, N. A. Lewinski, A. J. Coughlin, Y. Hu, E. S. Day, J. L. West and R. A. Drezek, *Small*, 2011, **7**, 169–183.
5 Z. Zhang, J. Wang, X. Nie, T. Wen, Y. Ji, X. Wu, Y. Zhao and C. Chen, *J. Am. Chem. Soc.*, 2014, **136**, 7317–7326.
6 T.-S. Deng, J. E. S. van der Hoeven, A. O. Yalcin, H. W. Zandbergen, M. A. van Huis and A. van Blaaderen, *Chem. Mater.*, 2015, **27**, 7196–7203.
7 C. Gao, Y. Hu, M. Wang, M. Chi and Y. Yin, *J. Am. Chem. Soc.*, 2014, **136**, 7474–7479.
8 D. Rioux, S. Vallières, S. Besner, P. Muñoz, E. Mazur and M. Meunier, *Adv. Opt. Mater.*, 2014, **2**, 176–182.
9 D. I. Enache, J. K. Edwards, P. Landon, B. Solsona-Espriu, A. F. Carley, A. A. Herzing, M. Watanabe, C. J. Kiely, D. W. Knight and G. J. Hutchings, *Science*, 2006, **311**, 362–365.
10 P. C. Chen, G. Liu, Y. Zhou, K. A. Brown, N. Chernyak, J. L. Hedrick, S. He, Z. Xie, Q. Y. Lin, V. P. Dravid, S. A. O'Neill-Slawecki and C. A. Mirkin, *J. Am. Chem. Soc.*, 2015, **137**, 9167–9173.
11 A. Wittstock, V. Zielasek, J. Biener, C. M. Friend and M. Bäumer, *Science*, 2010, **327**, 319–322.
12 J. K. Edwards, B. E. Solsona, P. Landon, A. F. Carley, A. Herzing, C. J. Kiely and G. J. Hutchings, *J. Catal.*, 2005, **236**, 69–79.
13 F. Wang, C. Li, H. Chen, R. Jiang, L.-D. Sun, Q. Li, J. Wang, J. C. Yu and C.-H. Yan, *J. Am. Chem. Soc.*, 2013, **135**, 5588–5601.
14 X. Liu, A. Wang, X. Yang, T. Zhang, C. Y. Mou, D. S. Su and J. Li, *Chem. Mater.*, 2009, **21**, 410–418.
15 A. Cao and G. Veser, *Nat. Mater.*, 2010, **9**, 75–81.
16 H. M. Bok, K. L. Shuford, S. G. Kim, S. K. Kim and S. Park, *Langmuir*, 2009, **25**, 5266–5270.
17 J. Huang, Y. Zhu, C. Liu, Y. Zhao, Z. Liu, M. N. Hedhili, A. Fratalocchi and Y. Han, *Small*, 2015, **11**, 5214–5221.
18 J. Crespo, J. M. López-de-Luzuriaga, M. Monge, M. E. Olmos, M. Rodríguez-Castillo, B. Cormary, K. Soulantica, M. Sestu and A. Falqui, *Chem. Commun.*, 2015, **51**, 16691–16694.
19 Q. Liu, Z. Yan, N. L. Henderson, J. C. Bauer, D. W. Goodman, J. D. Batteas and R. E. Schaak, *J. Am. Chem. Soc.*, 2009, **131**, 5720–5721.
20 Y. Lu, Y. Jiang and W. Chen, *Nano Energy*, 2013, **2**, 836–844.
21 A. Henkel, A. Jakab, G. Brunklaus and C. Sönnichsen, *J. Phys. Chem. C*, 2009, **113**, 2200–2204.
22 C. Wang, S. Peng, R. Chan and S. Sun, *Small*, 2009, **5**, 567–570.
23 H. Petrova, J. Perez Juste, I. Pastoriza-Santos, G. V. Hartland, L. M. Liz-Marzán and P. Mulvaney, *Phys. Chem. Chem. Phys.*, 2006, **8**, 814–821.
24 S. W. Prescott and P. Mulvaney, *J. Appl. Phys.*, 2006, **99**, 123504.
25 S. Link, Z. L. Wang and M. A. El-Sayed, *J. Phys. Chem. B*, 1999, **103**, 3529–3533.
26 E. A. Coronado and G. C. Schatz, *J. Chem. Phys.*, 2003, **119**, 3926–3934.
27 M. S. Shore, J. Wang, A. C. Johnston-Peck, A. L. Oldenburg and J. B. Tracy, *Small*, 2011, **7**, 230–234.
28 P. Buffat and J.-P. Borel, *Phys. Rev. A*, 1976, **13**, 2287–2298.
29 L. J. Lewis, P. Jensen and J.-L. Barrat, *Phys. Rev. B*, 1997, **56**, 2248–2257.
30 C. Burda, X. Chen, R. Narayanan and M. A. El-Sayed, *Chem. Rev.*, 2005, **105**, 1025–1102.
31 G. Guisbiers, R. Mendoza-Cruz, L. Bazán-Díaz, J. J. Velázquez-Salazar, R. Mendoza-Perez, J. A. Robledo-Torres, J.-L. Rodriguez-Lopez, J. M. Montejano-Carrizales, R. L. Whetten and M. José-Yacamán, *ACS Nano*, 2016, **10**, 188–198.
32 E. Gergely-Fülöp, D. Zámbó and A. Deák, *Mater. Chem. Phys.*, 2014, **148**, 909–913.
33 W. Albrecht, T.-S. Deng, B. Goris, M. A. van Huis, S. Bals and A. van Blaaderen, *Nano Lett.*, 2016, **16**, 1818–1825.
34 J. Hu, W. Cai, H. Zeng, C. Li and F. Sun, *J. Phys.: Condens. Matter*, 2006, **18**, 5415–5423.
35 E. Ringe, C. J. DeSantis, S. M. Collins, M. Duchamp, R. E. Dunin-Borkowski, S. E. Skrabalak and P. A. Midgley, *Sci. Rep.*, 2015, **5**, 17431.
36 P. Zijlstra, J. W. M. Chon and M. Gu, *Opt. Express*, 2007, **15**, 12151–12160.
37 S. H. Joo, J. Y. Park, C.-K. Tsung, Y. Yamada, P. Yang and G. A. Somorjai, *Nat. Mater.*, 2009, **8**, 126–131.